



1 **Formation drivers and photochemical effects of CINO₂ in a coastal city of**
2 **Southeast China**

3 Gaojie Chen^{1,4,5}, Xiaolong Fan^{1,4}, Haichao Wang^{2*}, Yee Jun Tham³, Ziyi Lin^{1,4,5}, Xiaoting Ji^{1,4,5}, Lingling

4 Xu^{1,4}, Baoye Hu⁶, Jinsheng Chen^{1,4*}

5

6 ¹Center for Excellence in Regional Atmospheric Environment, Institute of Urban Environment, Chinese

7 Academy of Sciences, Xiamen 361021, China

8 ²School of Atmospheric Sciences, Sun Yat-sen University, Zhuhai 519082, China

9 ³School of Marine Sciences, Sun Yat-sen University, Zhuhai 519082, China

10 ⁴Fujian Key Laboratory of Atmospheric Ozone Pollution Prevention, Institute of Urban Environment,

11 Chinese Academy of Sciences, Xiamen 361021, China

12 ⁵University of Chinese Academy of Sciences, Beijing 100049, China

13 ⁶Minnan Normal University, Zhangzhou 363000, China

14

15 *Correspondence to: Jinsheng Chen (jschen@iue.ac.cn); Haichao Wang (wanghch27@mail.sysu.edu.cn).

16

17

18

19

20

21

22

23

24

25

26

27



28 **Abstract.** Nitryl chloride (ClNO_2) is an important precursor of chlorine (Cl) radical, significantly affecting
29 ozone (O_3) formation and photochemical oxidation. However, the key drivers of ClNO_2 production are not
30 fully understood. In this study, the field observations of ClNO_2 and related parameters were conducted in a
31 coastal city of Southeast China during the autumn of 2022, combining with machine learning and model
32 simulations to elucidate its key influencing factors and atmospheric impacts. Elevated concentrations of
33 ClNO_2 (> 500 ppt) were notably observed during nighttime in late autumn, accompanied by increased levels
34 of dinitrogen pentoxide (N_2O_5) and nitrate (NO_3^-). Nighttime concentrations of ClNO_2 peaked at 3.4 ppb,
35 while its daytime levels remained significant, reaching up to 100 ppt and sustaining at approximately 40 ppt
36 at noon. Machine learning and field observations identified nighttime N_2O_5 heterogeneous uptake as the
37 predominant pathway for ClNO_2 production, whereas NO_3^- photolysis contributed to its daytime generation.
38 Additionally, ambient temperature (T) and relative humidity (RH) emerged as primary meteorological
39 factors affecting ClNO_2 formation, mainly through their effects on thermal equilibrium and N_2O_5 hydrolysis
40 processes, respectively. Ultraviolet (UV) radiation was found to play a dual role in ClNO_2 concentrations
41 around noon. Box model simulations showed that under high ClNO_2 conditions, the rates of alkane
42 oxidation by Cl radical in the early morning exceeded those by OH radical. Consequently, VOC oxidation
43 by Cl radical contributed $\sim 19\%$ to RO_x production rates, thereby significantly impacting O_3 formation and
44 atmospheric oxidation capacity. This research enriched the understanding of ClNO_2 generation and loss
45 pathways, providing valuable insights for the regulation of photochemical pollution in coastal regions.

46

47

48

49

50

51

52

53

54

55

56

57

58



59

60 **1 Introduction**

61 Chlorine (Cl) radical, as an important atmospheric oxidant, can react with volatile organic compounds
62 (VOCs) to affect RO_x (including OH, HO₂, and RO₂) radicals and ozone (O₃) formation (Yi et al., 2023),
63 thereby perturbing atmospheric chemical components and air quality (Peng et al., 2021; Li et al., 2020). The
64 reaction rates between Cl radical and some alkanes were several orders of magnitude faster than those
65 involving OH radical (Atkinson et al., 2006). Furthermore, the related studies indicated that the production
66 rates of Cl radical in the early morning could significantly exceed the production rates of OH radical formed
67 via O₃ photolysis (Phillips et al., 2012; Tham et al., 2016), thereby enhancing the atmospheric oxidation
68 capacity.

69 Nitryl chloride (ClNO₂) is one of the major Cl radical precursors in the tropospheric atmosphere
70 (Thornton et al., 2010; Xue et al., 2015; Liu et al., 2017). It is mainly generated by the heterogeneous uptake
71 of dinitrogen pentoxide (N₂O₅) on chloride-containing aerosols (Finlayson-Pitts et al., 1989; Thornton et al.,
72 2010), among which N₂O₅ is produced through the equilibrium reaction with nitrogen dioxide (NO₂) and
73 nitrate (NO₃) radical. Since Osthoff et al. (2008) firstly detected over 1 ppb of ClNO₂ in the urban outflows
74 of America (Osthoff et al., 2008), significant production of ClNO₂ has been widely observed in the polluted
75 coastal and inland areas with abundant anthropogenic emissions and chloride sources, with concentrations
76 ranging from tenths of ppt to several ppb (Riedel et al., 2012; Mielke et al., 2013; Mielke et al., 2011;
77 Phillips et al., 2012; Bannan et al., 2015; Wang et al., 2016; Xia et al., 2020; Xia et al., 2021; Yun et al.,
78 2018a; Wang et al., 2022; Li et al., 2023). For the diurnal profile of ClNO₂, its concentrations generally
79 peaked and accumulated at midnight, then rapidly decreased to low levels due to strong photolysis after
80 sunrise (Ma et al., 2023; Mielke et al., 2011; Xia et al., 2020). However, elevated daytime concentrations of
81 ClNO₂ have been observed in field studies, mainly attributed to reduced photolysis rates under heavy cloud
82 or fog cover, as well as contributions from horizontal and vertical transport (Tham et al., 2016; Xia et al.,
83 2021; Jeong et al., 2019; Mielke et al., 2013; Bannan et al., 2015). Notably, the recent laboratory research
84 demonstrated that nitrate (NO₃⁻) photolysis can generate ClNO₂ alongside Cl₂ (Dalton et al., 2023), yet this
85 mechanism has not been confirmed under real atmospheric conditions.

86 At present, the observation studies of ClNO₂ focused on investigating its influencing factors, such as
87 the N₂O₅ uptake coefficient and the production yield of ClNO₂ (Thornton et al., 2003; Tham et al., 2018).
88 The field and laboratory studies have indicated that ClNO₂ production was mainly affected by ambient
89 temperature (T), relative humidity (RH), and particle components (e.g., chloride (Cl⁻), NO₃⁻, and liquid



90 water content) (Bertram and Thornton, 2009; Wang et al., 2023; Wang et al., 2020). In addition to
91 influencing factors, the photochemical effects of ClNO₂ photolysis have been extensively evaluated (Xue et
92 al., 2015; Xia et al., 2021; Tham et al., 2016). Cl radical released by ClNO₂ photolysis will oxidize VOCs to
93 promote the formation of RO₂ radical and O₃, greatly compensating for the underestimation of RO₂ radical and
94 O₃ generation in model simulations (Peng et al., 2021; Ma et al., 2023). The field measurements of ClNO₂
95 have been conducted in different atmospheric environments, while the key drivers of ClNO₂ chemistry were
96 still not well recognized. Moreover, it is pertinent to explore whether there are additional and unrecognized
97 sources of ClNO₂ beyond its heterogeneous generation from N₂O₅.

98 In this study, the comprehensive measurements of ClNO₂ and related parameters were conducted in a
99 coastal city of Southeast China during the autumn of 2022. Our research integrated field observations with
100 machine learning to reveal the key driving factors of ClNO₂ formation, particularly, investigating the
101 potential generation mechanisms of daytime ClNO₂. Additionally, we also assessed the photochemical
102 impacts of ClNO₂ based on a box model. Overall, this study underscored the important role of NO₃⁻ in the
103 ClNO₂ chemistry.

104

105 **2 Materials and methods**

106 **2.1 Field Measurements**

107 The intensive field measurements of ClNO₂, related precursors, and meteorological parameters from
108 October 9th to December 5th, 2022 were performed at an urban site (Institute of Urban Environment,
109 Chinese Academy of Sciences) in a coastal city (Xiamen) of Southeast China (Fig. S1). Here, ClNO₂, N₂O₅,
110 gaseous pollutants (volatile organic compounds (VOCs), NO_x, SO₂, CO, and O₃), aerosol mass
111 concentrations, ionic components, size distribution, and meteorological factors were simultaneously detected.
112 Meanwhile, an iodide-adduct time-of-flight chemical ionization mass spectrometer (I⁻-ToF-CIMS) was used
113 to measure ClNO₂ and N₂O₅. The principles and settings of I⁻-ToF-CIMS were similar with previous studies
114 (Ma et al., 2023; Yan et al., 2023). Detailed descriptions of this observation site and instruments have been
115 provided in previous work (Chen et al., 2024; Hu et al., 2022), Text S1, and Table S1. For the calibrations of
116 ClNO₂ and N₂O₅, ClNO₂ was produced by passing Cl₂ (6 ppm in N₂) through a moist mixture of sodium
117 nitrite (NaNO₂) and sodium chloride (NaCl) (Thaler et al., 2011; Wang et al., 2022), and N₂O₅ was
118 synthesized by the reactions of O₃ and excessive NO₂ (Tham et al., 2016; Wang et al., 2016). The
119 dependences of ClNO₂ and N₂O₅ sensitivities on relative humidity are presented in Fig. S2. The details of
120 ClNO₂ and N₂O₅ calibrations and uncertainty analysis are displayed in Text S2.



121 **2.2 Machine Learning model**

122 Here, the extreme gradient boosting (XGBoost) model coupling with the Shapely additive explanations
123 (SHAP) model (the XGBoost-SHAP model) was used to identify the key influencing factors of ClNO₂
124 formation. Meanwhile, the XGBoost model was applied to establish the predictive model of ClNO₂ based on
125 the observed data of gaseous precursors and meteorological factors; the SHAP model was employed to
126 evaluate the importance of each feature affecting the simulated concentrations of ClNO₂. Besides, the partial
127 dependence plot (PDP) analysis offers a visual representation of the marginal effect that the factors have on
128 the model's predicted outcome. It is based on the principle of stabilizing the values of non-target features,
129 and systematically altered the target feature's values according to the model's algorithmic framework to
130 derive the predicted values.

131 ClNO₂ concentrations served as the dependent variable, with trace gases (SO₂, CO, NO₂, NO, O₃, and
132 N₂O₅), PM_{2.5} and its inorganic compositions (NO₃⁻, SO₄²⁻, NH₄⁺, and Cl⁻), and meteorological parameters (T,
133 RH, UV, WS, WD, and BLH) acting as independent variables. The simulated ClNO₂ concentrations by the
134 XGBoost model were highly similar with the observed values ($R^2=0.91$), indicating the good performance of
135 the XGBoost model (Fig. S3). Detailed introductions and settings of the XGBoost-SHAP model are
136 provided in Text S3.

137 **2.3 The box model**

138 The observation-based model (OBM) was utilized to assess the impacts of ClNO₂ on photochemically
139 atmospheric oxidation. As delineated in earlier studies (Xue et al., 2015; Tham et al., 2016; Xia et al., 2021;
140 Peng et al., 2021; Peng et al., 2022), the Master Chemical Mechanism (MCM, version 3.3.1) was adopted,
141 and established chlorine chemistry mechanisms have been integrated. The Tropospheric Ultraviolet and
142 Visible Radiation (TUV) model was employed to determine the ClNO₂ photolysis rates (J_{ClNO_2}) under
143 clear sky scenarios, subsequently calibrating J_{ClNO_2} by measured J_{NO_2} values. A thorough exposition of
144 the box model configuration can be found in our previous publications (Liu et al., 2022b; Liu et al., 2022a)
145 and Text S4. Observation data, including ClNO₂, VOCs, HCHO, HONO, CO, O₃, NO, NO₂, SO₂, along with
146 meteorological factors as constraint were input into the box model at an hourly resolution (Table S2). Two
147 scenarios were examined: one representing observation-average conditions from October 9th to December
148 5th, the other reflecting a high ClNO₂ case observed on November 28th.

149 This study focused on elucidating the influence of ClNO₂ on the formation of RO_x radical and O₃. The
150 O₃ production rate minus the O₃ loss rate was used to calculate the net O₃ production rate (Eq. S1-3). The
151 AOC is calculated by the sum of the rates of CH₄, CO, and VOCs oxidized by atmospheric oxidants (O₃, OH,



152 Cl, and NO₃ radical) (Eq. S4) (Xue et al., 2015; Yi et al., 2023). Both scenarios were evaluated with and
153 without including ClNO₂ inputs to assess its impacts on these processes.

154

155 **3 Results and discussion**

156 **3.1. Overview of observations**

157 Fig. 1 displays the time series of ClNO₂, N₂O₅, and related parameters including O₃, NO_x, PM_{2.5}, Cl⁻,
158 NO₃⁻, and meteorological parameters during the autumn observation period. Our observation shows a
159 decline in T and UV values from October to November, with average RH values increasing from ~ 60% in
160 October to ~ 70% in November (excluding rainy days). During the entire measurement period, ClNO₂
161 concentrations exhibited significant variability, with elevated levels (> 500 ppt) frequently observed in late
162 autumn, particularly after November 10th. The elevation of ClNO₂ concentrations coincided with increased
163 levels of N₂O₅ and NO₃⁻ during late autumn. The concentrations of ClNO₂ at our study site reached several
164 ppb, compared with previous field measurements conducted at urban, suburban, rural, background, and
165 mountain sites (Table S3), indicating its widespread presence in diverse atmospheric environments. The
166 highest concentrations of ClNO₂ were detected at midnight of November 27th, with maximum hourly
167 average concentrations of 3.4 ppb. Simultaneously, peak concentrations of N₂O₅ and NO₃⁻ were also
168 observed (Fig. 1). On the evening of November 27th, N₂O₅ concentrations rapidly decreased after 7 p.m.,
169 while ClNO₂ and NO₃⁻ concentrations significantly increased, reflecting fast N₂O₅ heterogeneous hydrolysis
170 and effective formation of ClNO₂. Notably, on the following day (November 28th) (Fig. 2a), ClNO₂
171 concentrations sustained above 100 ppt around noon, partially related with weaken UV values (~ 14 W·m⁻²)
172 under heavy fog and cloud cover, with the RH values of ~ 70% at that time. Similar research in California
173 has shown ClNO₂ concentrations exceeding 100 ppt after sunrise 4 hours due to reduced photolysis (Mielke
174 et al., 2013).

175 The average diurnal changes of ClNO₂ and related parameters during the entire measurement campaign
176 were depicted in Fig. 2b. As expected, ClNO₂ exhibited a distinct diurnal variation, peaking and
177 accumulating after sunset and decreasing in the early morning. However, ClNO₂ concentrations remained ~
178 40 ppt around noon, different with some studies that ClNO₂ concentrations decreased to near the detection
179 limit around midday (Wang et al., 2022; Niu et al., 2022). N₂O₅ concentrations only presented a small peak
180 after sunset, and declined to near the detection limit in the daytime, suggesting minimal contribution from
181 daytime ClNO₂ formation via N₂O₅ heterogeneous uptake. Similar observation in North China declared
182 ClNO₂ concentrations above 60 ppt in the afternoon (Liu et al., 2017). Previous studies have indicated that



183 abundant ClNO₂ may be transported from upper atmosphere or air mass, contributing to the elevated ClNO₂
184 concentrations in the early morning (Tham et al., 2016; Xia et al., 2021; Jeong et al., 2019). However, the
185 explanations for the concentrations of ClNO₂ around noon remained elusive, implying additional sources
186 driving daytime ClNO₂ generation beyond N₂O₅ uptake.

187 **3.2. Key drivers of ClNO₂ formation**

188 The XGBoost-SHAP model was employed to investigate the major drivers of ClNO₂ production during
189 the whole observation period. The average absolute SHAP value of each feature was ranked to determine the
190 key drivers of ClNO₂ formation, with larger SHAP values suggesting greater contributions (Fig. 3a).
191 Additionally, features with positive SHAP values (depicted as red points) indicate that higher values of those
192 features positively affect ClNO₂ concentrations, and vice versa (Fig. 3b). Overall, N₂O₅, NO₃⁻, T, RH, and
193 UV were the most important features affecting ClNO₂ concentrations. Notably, these factors exhibited varied
194 behaviors between daytime and nighttime periods (Fig. 5).

195 In our study, N₂O₅ was identified as the most important influencing factor, consistent with its role in
196 ClNO₂ formation through heterogeneous uptake processes (Thornton et al., 2010; Finlayson-Pitts et al.,
197 1989). After sunset, ClNO₂ concentrations markedly increased due to active nighttime N₂O₅ chemistry,
198 while this heterogeneous uptake process was hindered after sunrise as N₂O₅ concentrations decreased
199 significantly (Fig. 1) (Niu et al., 2022; Wang et al., 2020; Tan et al., 2022). Indeed, the concentrations of
200 ClNO₂ were evidently increased when N₂O₅ concentrations exceeded ~13 ppt, predominantly during the
201 nighttime (Fig. 4a). Conversely, in Northern Europe, the ClNO₂ concentrations were mainly controlled by
202 O₃ and NO₂, rather than by the heterogeneous uptake of N₂O₅ (Sommariva et al., 2018). In Heshan of South
203 China, chloride and PM_{2.5} were the major factors affecting ClNO₂ formation (Wang et al., 2022). Differently,
204 NO₃⁻ could play a vital role in affecting the concentrations of ClNO₂ alongside N₂O₅ in this study.
205 According to Fig. 4b, the high NO₃⁻ concentrations (> 3.7 μg·m⁻³) corresponded to the elevation of ClNO₂,
206 especially its concentrations exceeding 6.2 μg·m⁻³. It is well recognized that NO₃⁻ and ClNO₂ were co-
207 products from the processes of N₂O₅ heterogeneous uptake (Wang et al., 2017; Yun et al., 2018b). Hence, the
208 relative importance of NO₃⁻ derived from the XGBoost-SHAP result indicated that the process of NO₃⁻
209 formation is accompanied by the generation of ClNO₂ at night during our observation period. As mentioned
210 before, it is evidently observed that elevated concentrations of nighttime ClNO₂ were coincided with
211 increased NO₃⁻ concentrations in late autumn. Considering the limited contribution of N₂O₅ hydrolysis to
212 daytime NO₃⁻ levels (Yan et al., 2023; Zang et al., 2022; Chen et al., 2020), the impact of high NO₃⁻
213 concentrations on daytime ClNO₂ concentrations warrants further analysis.



214 The simulated concentrations of ClNO_2 , based on the XGBoost-SHAP model, were significantly
215 elevated when NO_3^- concentrations were higher than $3.7 \mu\text{g}\cdot\text{m}^{-3}$ (Fig. 4b). Consequently, the averaged daily
216 concentrations of NO_3^- were classified as high ($> 3.7 \mu\text{g}\cdot\text{m}^{-3}$) and low ($< 3.7 \mu\text{g}\cdot\text{m}^{-3}$) to further elucidate the
217 impacts of NO_3^- on the formation of ClNO_2 . Fig. 5 presents the diurnal variations in the relative importance
218 of factors based on the SHAP values under high and low NO_3^- concentrations. Unexpectedly, daytime NO_3^-
219 was the dominant influencing factors for daytime ClNO_2 (Fig. 5a). High concentrations of daytime NO_3^-
220 positively affected the daytime concentrations of ClNO_2 , independent of N_2O_5 uptake processes. As depicted
221 in Fig. 5a, daytime N_2O_5 did not promote the elevation of daytime ClNO_2 . Therefore, it is very likely that
222 high concentrations of daytime NO_3^- participated in daytime ClNO_2 production. A recent study declared that
223 nitrate photolysis produced ClNO_2 in addition to Cl_2 (Dalton et al., 2023), while it has been not verified by
224 field observations. Fig. 6 shows that daytime ClNO_2 concentrations correlated well ($R=0.62$) with the
225 product of a proxy of NO_3^- photolysis ($\text{NO}_3^- \times J\text{NO}_2 \times S_a$) on aerosol surfaces (S_a), implying that the
226 photolysis of NO_3^- contributed to the daytime concentrations of ClNO_2 at our study site. Furthermore, high
227 concentrations of NO_3^- and Cl^- , along with large values of S_a (Fig. 6a, b, c) in the daytime accelerated NO_3^-
228 photolysis, promoting the formation of ClNO_2 . Overall, N_2O_5 uptake processes were the major pathways
229 dominating nighttime ClNO_2 formation, while NO_3^- photolysis contributed to daytime ClNO_2 production
230 during our observation period.

231 In terms of meteorological factors, UV, T, and RH were the major influencing factors. The photolysis
232 was the most important sink of ClNO_2 in the daytime, leading to a rapid reduction in ClNO_2 concentrations,
233 particularly in the early morning (Fig. 4e and Fig. 5). The weakened UV from October to November
234 decreased the photolysis rate of ClNO_2 (Fig. 1a), while NO_3^- photolysis contributed partially to daytime
235 ClNO_2 concentrations (Fig. 6d), indicating the dual role of photolysis (or UV). The impact of T on ClNO_2
236 was probably reflected in its thermal equilibrium with N_2O_5 . Elevated daytime T inhibited the formation of
237 N_2O_5 (Fig. 4c and Fig. 5). During the whole observation period from October to November, the drop in T
238 facilitated ClNO_2 production by decreasing the thermal decomposition process (Fig. 5). Increased RH values
239 provided favorable conditions for the nighttime N_2O_5 hydrolysis reactions, thereby affecting ClNO_2
240 production (Fig. 4d and Fig. 5), while high RH ($> 80\%$) also weakened the generation of ClNO_2 . Notably,
241 Cl^- was not the most important factors of ClNO_2 formation at our study site (Fig. 3), likely attributed to the
242 abundant chlorine source in coastal regions (Peng et al., 2022).

243 3.3. Photochemical effects of ClNO_2

244 The photochemical effects of ClNO_2 were evaluated under the observation-average condition and the



245 high ClNO₂ case based on the box model. The largest Cl production rates (P(Cl)) contributed from ClNO₂
246 photolysis were 0.05 ppb·h⁻¹ for the observation-average condition, which was lower than 0.19 ppb·h⁻¹ for
247 the high ClNO₂ case. The difference led to variable levels of atmospheric oxidation capacity induced by Cl
248 radical. Cl radical released via the photolysis of ClNO₂ initiated the oxidation of VOCs. Among VOC
249 groups (including alkanes, alkenes, alkynes, aromatics and OVOCs), Cl radical primarily oxidized alkanes
250 (~ 65.0%), followed by OVOCs (~ 12.7%) for both the observation-average condition and the high ClNO₂
251 case (Fig. 7a, b). The contributions of Cl radical and other atmospheric oxidants (including OH radical and
252 O₃) to daytime VOC oxidation were also compared (Fig. 7c, d and Table 1). In our study, the oxidation of
253 alkanes by Cl radical for the observation-average condition were about 11.7%, which increased by 44.8%
254 for the high ClNO₂ case, were higher than those in London (Bannan et al., 2015), Weybourne (Bannan et al.,
255 2017), Boston (Rutherford et al., 1995), and LA (Fraser et al., 1997), lower than that in Hong Kong (Xue et
256 al., 2015). It should be noticed that the rates of Cl radical reacting with alkanes even exceeded those of OH
257 radical in the early morning for the high ClNO₂ case. The largest rates of alkanes oxidized by Cl radical were
258 approximately twice as high as those of OH radical at 10 a.m. (Fig. 7e, f), highlighting that the
259 photochemical effects of Cl radical released via ClNO₂ photolysis were particularly important for VOC
260 oxidation during the morning hours at our study site.

261 The oxidation of VOCs by Cl radical further affects the generation of RO_x (OH + HO₂ + RO₂) radicals.
262 The RO_x radical production rates for the high ClNO₂ case were evidently lower than that under the
263 observation-average condition, primarily due to reduced photolysis rates on that day. However, the total RO_x
264 radical production rates averagely increased by 23.8% with ClNO₂ photolysis for the high ClNO₂ case,
265 higher than a 4.9% increase for the observation-average condition (Fig. S4). For the observation-average
266 condition, O₃ (32.7%), HONO (31.7%), and OVOCs (21.6%) photolysis were the most significant
267 contributors to RO_x radical production in the early morning (7-10 a.m.), with VOC oxidation by Cl radical
268 contributing only 3.7% (Fig. 8a). However, for the high ClNO₂ case, VOC oxidation induced by Cl radical
269 in the early morning accounted for 19.1% of RO_x radical production, which was higher than O₃ (7.4%) and
270 HCHO (4.1%) photolysis, close to OVOCs (19.0%) photolysis (Fig. 8b). The contributions of ClNO₂
271 photolysis to the RO_x radical production rates in our study were larger than previous results observed in
272 autumn of Heshan (Wang et al., 2022) and North China (Xia et al., 2021), similar with that in summer of
273 Wangdu (Tham et al., 2016). Thus, the concentrations of OH, HO₂, and RO₂ radicals in the box model with
274 ClNO₂ inputs averagely increased by 17.9%, 34.6%, and 54.3% for the high ClNO₂ case, higher than the
275 increases of 3.7%, 7.1%, and 10.3% contributed from the observation-average conditions, respectively (Fig.



276 S5). The uplift in the concentrations of RO_x radicals also accelerated the generation of O_3 . The increase in
277 the net O_3 production rates ($P(\text{O}_3)$) for the observation-average condition averagely reached $0.13 \text{ ppb}\cdot\text{h}^{-1}$
278 (15.8 %) in the daytime (Fig. 9a), while larger elevations in the net $P(\text{O}_3)$ were observed for the high ClNO_2
279 case (Fig. 9b), with a maximum of $0.64 \text{ ppb}\cdot\text{h}^{-1}$ (120 %) at 10 a.m. As a result, increased RO_x radical and O_3
280 greatly enhanced the atmospheric oxidation capacity (Fig. 9c, d), especially for the high ClNO_2 case (up to
281 65%).

282 Table 2 summarizes the impacts of ClNO_2 photolysis on RO_x radical and O_3 production in our study
283 and previous observations around the world (Xia et al., 2021; Wang et al., 2022; Tham et al., 2016; Wang et
284 al., 2016; Xue et al., 2015; Bannan et al., 2017; Jeong et al., 2019), indicating that the photochemical
285 impacts of ClNO_2 were variable in different atmospheric environments. At our study site, the effects of
286 ClNO_2 photolysis on RO_x radical production were important, especially in the early morning. The enhanced
287 RO_x radical production induced by ClNO_2 photolysis accelerated the chemical generation of O_3 . Primary
288 RO_x radical production rates (including O_3 , HONO, HCHO, OVOCs, and ClNO_2) were considered as one of
289 the most important parameters to O_3 formation (Lu et al., 2023). Therefore, the considerable contribution of
290 ClNO_2 photolysis to primary RO_x radical production in the early morning may bring new challenges for O_3
291 alleviation.

292

293 Conclusions

294 In conclusion, we present two months of field measurements in the coastal area of Southern China
295 during the autumn, coupled with machine learning and model simulations, providing new insights into
296 ClNO_2 chemistry. Our observation shows the increase in the concentrations of ClNO_2 were accompanied by
297 elevated concentrations of N_2O_5 and NO_3^- , low values of T and UV, and high values of RH. The nighttime
298 heterogeneous uptake of N_2O_5 was identified as the major source of ClNO_2 , while NO_3^- photolysis
299 promoted the elevation of daytime ClNO_2 concentrations. Cl radical released by ClNO_2 photolysis after
300 sunrise had important photochemical effects in the early morning. The photolysis of high ClNO_2
301 concentrations resulted in net O_3 production rates and atmospheric oxidation capacity levels increasing by
302 120% and 65%, respectively. Our results enhanced the understanding of ClNO_2 chemistry in coastal regions,
303 calling for more observations and laboratory research to fully reveal its exact role in different atmospheric
304 environments.

305

306 **Data availability.** Data are available upon request to Jinsheng Chen (jschen@iue.ac.cn).



307

308 **Author contributions.** JC provided funding support for field measurements, designed this study, and
309 revised this manuscript. GC designed this study, analyzed the data, and wrote this manuscript. HW helped
310 perform the calibrations and revised this manuscript. XF revised this manuscript. XF, HW, YT, ZL, XJ, LX,
311 BH contributed to discussions of this manuscript.

312

313 **Competing interests.** The authors declare that they have no conflict of interest.

314

315 **Acknowledgements.** The authors acknowledge the National Natural Science Foundation of China, the
316 Science and Technology Department of Fujian Province, Center for Excellence in Regional Atmospheric
317 Environment Project, Xiamen Atmospheric Environment Observation and Research Station of Fujian
318 Province, and Fujian Key Laboratory of Atmospheric Ozone Pollution Prevention (Institute of Urban
319 Environment, Chinese Academy of Sciences).

320

321 **Financial support.** This work was funded by the National Natural Science Foundation of China
322 (U22A20578, 42305102 & 42277091), the Science and Technology Department of Fujian Province
323 (2022L3025), the National Key Research and Development Program (2022YFC3700304), STS Plan
324 Supporting Project of the Chinese Academy of Sciences in Fujian Province (2023T3013), Fujian Provincial
325 Environmental Protection Science & Technology Plan Projects (2023R004), and Xiamen Atmospheric
326 Environment Observation and Research Station of Fujian Province. Y.J.T. acknowledges the funding support
327 from the Guangdong Basic and Applied Basic Research Foundation (2022A1515010852) and the
328 Fundamental Research Funds for the Central Universities, Sun Yat-sen University (23hytd002).

329

330 **References**

331 Atkinson, R., Baulch, D. L., Cox, R. A., Crowley, J. N., Hampson, R. F., Hynes, R. G., Jenkin, M. E., Rossi,
332 M. J., Troe, J., and Subcommittee, I.: Evaluated kinetic and photochemical data for atmospheric chemistry:
333 Volume II – gas phase reactions of organic species, *Atmos. Chem. Phys.*, 6, 3625-4055,
334 <https://doi.org/10.5194/acp-6-3625-2006>, 2006.

335 Bannan, T. J., Bacak, A., Le Breton, M., Flynn, M., Ouyang, B., McLeod, M., Jones, R., Malkin, T. L.,



- 336 Whalley, L. K., Heard, D. E., Bandy, B., Khan, M. A. H., Shallcross, D. E., and Percival, C. J.: Ground and
337 Airborne U.K. Measurements of Nitryl Chloride: An Investigation of the Role of Cl Atom Oxidation at
338 Weybourne Atmospheric Observatory, *J. Geophys. Res. Atmos.*, 122, 11,154-111,165,
339 <https://doi.org/10.1002/2017jd026624>, 2017.
- 340 Bannan, T. J., Booth, A. M., Bacak, A., Muller, J. B. A., Leather, K. E., Le Breton, M., Jones, B., Young, D.,
341 Coe, H., Allan, J., Visser, S., Slowik, J. G., Furger, M., Prévôt, A. S. H., Lee, J., Dunmore, R. E., Hopkins, J.
342 R., Hamilton, J. F., Lewis, A. C., Whalley, L. K., Sharp, T., Stone, D., Heard, D. E., Fleming, Z. L., Leigh,
343 R., Shallcross, D. E., and Percival, C. J.: The first UK measurements of nitryl chloride using a chemical
344 ionization mass spectrometer in central London in the summer of 2012, and an investigation of the role of Cl
345 atom oxidation, *J. Geophys. Res. Atmos.*, 120, 5638-5657, <https://doi.org/10.1002/2014jd022629>, 2015.
- 346 Bertram, T. and Thornton, J.: Toward a general parameterization of N₂O₅ reactivity on aqueous particles: the
347 competing effects of particle liquid water, nitrate and chloride, *Atmos. Chem. Phys.*, 9, 8351-8363,
348 <https://doi.org/10.5194/acp-9-8351-2009>, 2009.
- 349 Chen, G., Ji, X., Chen, J., Xu, L., Hu, B., Lin, Z., Fan, X., Li, M., Hong, Y., and Chen, J.: Photochemical
350 pollution during summertime in a coastal city of Southeast China: Ozone formation and influencing factors,
351 *Atmos. Res.*, 301, 107270, <https://doi.org/10.1016/j.atmosres.2024.107270>, 2024.
- 352 Chen, X., Wang, H., Lu, K., Li, C., Zhai, T., Tan, Z., Ma, X., Yang, X., Liu, Y., Chen, S., Dong, H., Li, X.,
353 Wu, Z., Hu, M., Zeng, L., and Zhang, Y.: Field Determination of Nitrate Formation Pathway in Winter
354 Beijing, *Environ. Sci. Technol.*, 54, 9243-9253, <https://doi.org/10.1021/acs.est.0c00972>, 2020.
- 355 Dalton, E. Z., Hoffmann, E. H., Schaefer, T., Tilgner, A., Herrmann, H., and Raff, J. D.: Daytime
356 Atmospheric Halogen Cycling through Aqueous-Phase Oxygen Atom Chemistry, *J. Am. Chem. Soc.*, 145,
357 15652-15657, <https://doi.org/10.1021/jacs.3c03112>, 2023.
- 358 Finlayson-Pitts, B. J., Ezell, M. J., and Pitts, J. N.: Formation of chemically active chlorine compounds by
359 reactions of atmospheric NaCl particles with gaseous N₂O₅ and ClONO₂, *Nature.*, 337, 241-244,
360 <https://doi.org/10.1038/337241a0>, 1989.
- 361 Fraser, M. P., Cass, G. R., Simoneit, B. R., and Rasmussen, R.: Air quality model evaluation data for
362 organics. 4. C₂-C₃₆ non-aromatic hydrocarbons, *Environ. Sci. Technol.*, 31, 2356-2367,



- 363 <https://doi.org/10.1021/es960980g>, 1997.
- 364 Hu, B., Duan, J., Hong, Y., Xu, L., Li, M., Bian, Y., Qin, M., Fang, W., Xie, P., and Chen, J.: Exploration of
365 the atmospheric chemistry of nitrous acid in a coastal city of southeastern China: results from measurements
366 across four seasons, *Atmos. Chem. Phys.*, 22, 371-393, <https://doi.org/10.5194/acp-22-371-2022>, 2022.
- 367 Jeong, D., Seco, R., Gu, D., Lee, Y., Nault, B. A., Knote, C. J., McGee, T., Sullivan, J. T., Jimenez, J. L.,
368 Campuzano-Jost, P., Blake, D. R., Sanchez, D., Guenther, A. B., Tanner, D., Huey, L. G., Long, R.,
369 Anderson, B. E., Hall, S. R., Ullmann, K., Shin, H., Herndon, S. C., Lee, Y., Kim, D., Ahn, J., and Kim, S.:
370 Integration of airborne and ground observations of nitryl chloride in the Seoul metropolitan area and the
371 implications on regional oxidation capacity during KORUS-AQ 2016, *Atmos. Chem. Phys.*, 19, 12779-
372 12795, <https://doi.org/10.5194/acp-19-12779-2019>, 2019.
- 373 Li, F., Huang, D. D., Nie, W., Tham, Y. J., Lou, S., Li, Y., Tian, L., Liu, Y., Zhou, M., and Wang, H.:
374 Observation of nitrogen oxide-influenced chlorine chemistry and source analysis of Cl₂ in the Yangtze River
375 Delta, China, *Atmos. Environ.*, 306, 119829, <https://doi.org/10.1016/j.atmosenv.2023.119829>, 2023.
- 376 Li, Q., Badia, A., Wang, T., Sarwar, G., Fu, X., Zhang, L., Zhang, Q., Fung, J., Cuevas, C. A., Wang, S.,
377 Zhou, B., and Saiz-Lopez, A.: Potential Effect of Halogens on Atmospheric Oxidation and Air Quality in
378 China, *J. Geophys. Res. Atmos.*, 125, e2019JD032058, <https://doi.org/10.1029/2019JD032058>, 2020.
- 379 Liu, T., Chen, G., Chen, J., Xu, L., Li, M., Hong, Y., Chen, Y., Ji, X., Yang, C., Chen, Y., Huang, W., Huang,
380 Q., and Wang, H.: Seasonal characteristics of atmospheric peroxyacetyl nitrate (PAN) in a coastal city of
381 Southeast China: Explanatory factors and photochemical effects, *Atmos. Chem. Phys.*, 22, 4339-4353,
382 <https://doi.org/10.5194/acp-22-4339-2022>, 2022a.
- 383 Liu, T., Hong, Y., Li, M., Xu, L., Chen, J., Bian, Y., Yang, C., Dan, Y., Zhang, Y., Xue, L., Zhao, M., Huang,
384 Z., and Wang, H.: Atmospheric oxidation capacity and ozone pollution mechanism in a coastal city of
385 southeastern China: analysis of a typical photochemical episode by an observation-based model, *Atmos.*
386 *Chem. Phys.*, 22, 2173-2190, <https://doi.org/10.5194/acp-22-2173-2022>, 2022b.
- 387 Liu, X., Qu, H., Huey, L. G., Wang, Y., Sjostedt, S., Zeng, L., Lu, K., Wu, Y., Hu, M., Shao, M., Zhu, T., and
388 Zhang, Y.: High Levels of Daytime Molecular Chlorine and Nitryl Chloride at a Rural Site on the North
389 China Plain, *Environ. Sci. Technol.*, 51, 9588-9595, <https://doi.org/10.1021/acs.est.7b03039>, 2017.



- 390 Lu, K., Zhou, H., Lee, J., Nelson, B., and Zhang, Y.: Ozone mitigations beyond the control of nitrogen
391 oxides and volatile organic compounds, *Sci Bull*, 68, 1989-1992, <https://doi.org/10.1016/j.scib.2023.07.051>,
392 2023.
- 393 Ma, W., Chen, X., Xia, M., Liu, Y., Wang, Y., Zhang, Y., Zheng, F., Zhan, J., Hua, C., and Wang, Z.:
394 Reactive Chlorine Species Advancing the Atmospheric Oxidation Capacities of Inland Urban Environments,
395 *Environ. Sci. Technol.*, 57, 14638-14647, <https://doi.org/10.1021/acs.est.3c05169>, 2023.
- 396 Mielke, L. H., Furgeson, A., and Osthoff, H. D.: Observation of ClNO₂ in a Mid-Continental Urban
397 Environment, *Environ. Sci. Technol.*, 45, 8889-8896, <https://doi.org/10.1021/es201955u>, 2011.
- 398 Mielke, L. H., Stutz, J., Tsai, C., Hurlock, S. C., Roberts, J. M., Veres, P. R., Froyd, K. D., Hayes, P. L.,
399 Cubison, M. J., Jimenez, J. L., Washenfelder, R. A., Young, C. J., Gilman, J. B., Gouw, J. A., Flynn, J. H.,
400 Grossberg, N., Lefer, B. L., Liu, J., Weber, R. J., and Osthoff, H. D.: Heterogeneous formation of nitryl
401 chloride and its role as a nocturnal NO_x reservoir species during CalNex-LA 2010, *J. Geophys. Res. Atmos.*,
402 118, 10,638-610,652, <https://doi.org/10.1002/jgrd.50783>, 2013.
- 403 Niu, Y.-B., Zhu, B., He, L.-Y., Wang, Z., Lin, X.-Y., Tang, M.-X., and Huang, X.-F.: Fast Nocturnal
404 Heterogeneous Chemistry in a Coastal Background Atmosphere and Its Implications for Daytime
405 Photochemistry, *J. Geophys. Res. Atmos.*, 127, e2022JD036716, <https://doi.org/10.1029/2022JD036716>,
406 2022.
- 407 Osthoff, H. D., Roberts, J. M., Ravishankara, A. R., Williams, E. J., Lerner, B. M., Sommariva, R., Bates, T.
408 S., Coffman, D., Quinn, P. K., Dibb, J. E., Stark, H., Burkholder, J. B., Talukdar, R. K., Meagher, J.,
409 Fehsenfeld, F. C., and Brown, S. S.: High levels of nitryl chloride in the polluted subtropical marine
410 boundary layer, *Nat. Geosci.*, 1, 324-328, <https://doi.org/10.1038/ngeo177>, 2008.
- 411 Peng, X., Wang, T., Wang, W., Ravishankara, A., George, C., Xia, M., Cai, M., Li, Q., Salvador, C. M., and
412 Lau, C.: Photodissociation of particulate nitrate as a source of daytime tropospheric Cl₂, *Nat. Commun.*, 13,
413 1-10, <https://doi.org/10.1038/s41467-022-28383-9>, 2022.
- 414 Peng, X., Wang, W., Xia, M., Chen, H., Ravishankara, A. R., Li, Q., Saiz-Lopez, A., Liu, P., Zhang, F.,
415 Zhang, C., Xue, L., Wang, X., George, C., Wang, J., Mu, Y., Chen, J., and Wang, T.: An unexpected large
416 continental source of reactive bromine and chlorine with significant impact on wintertime air quality, *Natl.*



- 417 Sci. Rev., 8, nwaa304, <https://doi.org/10.1093/nsr/nwaa304>, 2021.
- 418 Phillips, G. J., Tang, M. J., Thieser, J., Brickwedde, B., Schuster, G., Bohn, B., Lelieveld, J., and Crowley, J.
419 N.: Significant concentrations of nitryl chloride observed in rural continental Europe associated with the
420 influence of sea salt chloride and anthropogenic emissions, *Geophys. Res. Lett.*, 39, L10811,
421 <https://doi.org/10.1029/2012gl051912>, 2012.
- 422 Riedel, T. P., Bertram, T. H., Crisp, T. A., Williams, E. J., Lerner, B. M., Vlasenko, A., Li, S. M., Gilman, J.,
423 de Gouw, J., Bon, D. M., Wagner, N. L., Brown, S. S., and Thornton, J. A.: Nitryl chloride and molecular
424 chlorine in the coastal marine boundary layer, *Environ. Sci. Technol.*, 46, 10463-10470,
425 <https://doi.org/10.1021/es204632r>, 2012.
- 426 Rutherford, J. A., Koehl, W. J., Benson, J. D., Burns, V. R., Hochhauser, A. M., Knepper, J. C., Leppard, W.
427 R., Painter, L. J., Rapp, L. A., and Rippon, B.: Effects of Gasoline Properties on Emissions of Current and
428 Future Vehicles-T50, T90, and Sulfur Effects-Auto/Oil Air Quality Improvement Research Program, SAE
429 Technical Paper0148-7191, <https://doi.org/10.4271/952510>, 1995.
- 430 Sommariva, R., Hollis, L. D. J., Sherwen, T., Baker, A. R., Ball, S. M., Bandy, B. J., Bell, T. G., Chowdhury,
431 M. N., Cordell, R. L., Evans, M. J., Lee, J. D., Reed, C., Reeves, C. E., Roberts, J. M., Yang, M., and Monks,
432 P. S.: Seasonal and geographical variability of nitryl chloride and its precursors in Northern Europe, *Atmos.*
433 *Sci. Lett.*, 19, <https://doi.org/10.1002/asl.844>, 2018.
- 434 Tan, Z., Fuchs, H., Hofzumahaus, A., Bloss, W. J., Bohn, B., Cho, C., Hohaus, T., Holland, F., Lakshmisha,
435 C., Liu, L., Monks, P. S., Novelli, A., Niether, D., Rohrer, F., Tillmann, R., Valkenburg, T. S. E., Vardhan, V.,
436 Kiendler-Scharr, A., Wahner, A., and Sommariva, R.: Seasonal variation in nitryl chloride and its relation to
437 gas-phase precursors during the JULIAC campaign in Germany, *Atmos. Chem. Phys.*, 22, 13137-13152,
438 <https://doi.org/10.5194/acp-22-13137-2022>, 2022.
- 439 Thaler, R. D., Mielke, L. H., and Osthoff, H. D.: Quantification of nitryl chloride at part per trillion mixing
440 ratios by thermal dissociation cavity ring-down spectroscopy, *Anal. Chem.*, 83, 2761-2766,
441 <https://doi.org/10.1021/ac200055z>, 2011.
- 442 Tham, Y. J., Wang, Z., Li, Q., Wang, W., Wang, X., Lu, K., Ma, N., Yan, C., Kecorius, S., Wiedensohler, A.,
443 Zhang, Y., and Wang, T.: Heterogeneous N₂O₅ uptake coefficient and production yield of ClNO₂ in polluted



444 northern China: roles of aerosol water content and chemical composition, *Atmos. Chem. Phys.*, 18, 13155-
445 13171, <https://doi.org/10.5194/acp-18-13155-2018>, 2018.

446 Tham, Y. J., Wang, Z., Li, Q., Yun, H., Wang, W., Wang, X., Xue, L., Lu, K., Ma, N., Bohn, B., Li, X.,
447 Kecorius, S., Größ, J., Shao, M., Wiedensohler, A., Zhang, Y., and Wang, T.: Significant concentrations of
448 nitryl chloride sustained in the morning: investigations of the causes and impacts on ozone production in a
449 polluted region of northern China, *Atmos. Chem. Phys.*, 16, 14959-14977, [https://doi.org/10.5194/acp-16-](https://doi.org/10.5194/acp-16-14959-2016)
450 [14959-2016](https://doi.org/10.5194/acp-16-14959-2016), 2016.

451 Thornton, J. A., Braban, C. F., and Abbatt, J. P.: N₂O₅ hydrolysis on sub-micron organic aerosols: the effect
452 of relative humidity, particle phase, and particle size, *Phys. Chem. Chem. Phys.*, 5, 4593-4603,
453 <https://doi.org/10.1039/B307498F>, 2003.

454 Thornton, J. A., Kercher, J. P., Riedel, T. P., Wagner, N. L., Cozic, J., Holloway, J. S., Dubé, W. P., Wolfe, G.
455 M., Quinn, P. K., Middlebrook, A. M., Alexander, B., and Brown, S. S.: A large atomic chlorine source
456 inferred from mid-continental reactive nitrogen chemistry, *Nature.*, 464, 271-274,
457 <https://doi.org/10.1038/nature08905>, 2010.

458 Wang, H., Yuan, B., Zheng, E., Zhang, X., Wang, J., Lu, K., Ye, C., Yang, L., Huang, S., and Hu, W.:
459 Formation and impacts of nitryl chloride in Pearl River Delta, *Atmos. Chem. Phys.*, 22, 14837-14858,
460 <https://doi.org/10.5194/acp-22-14837-2022>, 2022.

461 Wang, H., Wang, H., Lu, X., Lu, K., Zhang, L., Tham, Y. J., Shi, Z., Aikin, K., Fan, S., Brown, S. S., and
462 Zhang, Y.: Increased night-time oxidation over China despite widespread decrease across the globe, *Nat.*
463 *Geosci.*, 16, 217-223, <https://doi.org/10.1038/s41561-022-01122-x>, 2023.

464 Wang, H., Chen, X., Lu, K., Tan, Z., Ma, X., Wu, Z., Li, X., Liu, Y., Shang, D., Wu, Y., Zeng, L., Hu, M.,
465 Schmitt, S., Kiendler-Scharr, A., Wahner, A., and Zhang, Y.: Wintertime N₂O₅ uptake coefficients over the
466 North China Plain, *Sci. Bull.*, 65, 765-774, <https://doi.org/10.1016/j.scib.2020.02.006>, 2020.

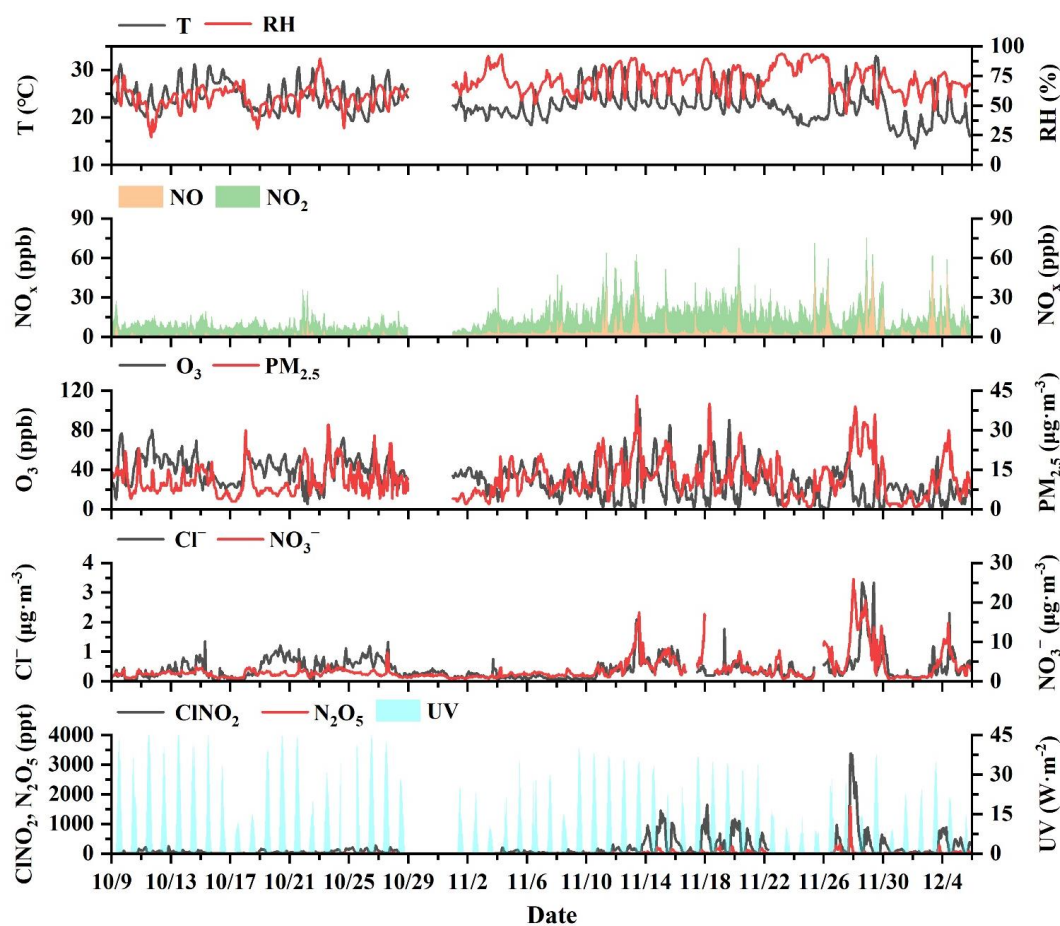
467 Wang, T., Tham, Y. J., Xue, L., Li, Q., Zha, Q., Wang, Z., Poon, S. C. N., Dubé, W. P., Blake, D. R., Louie, P.
468 K. K., Luk, C. W. Y., Tsui, W., and Brown, S. S.: Observations of nitryl chloride and modeling its source and
469 effect on ozone in the planetary boundary layer of southern China, *J. Geophys. Res. Atmos.*, 121, 2476-2489,
470 <https://doi.org/10.1002/2015JD024556>, 2016.



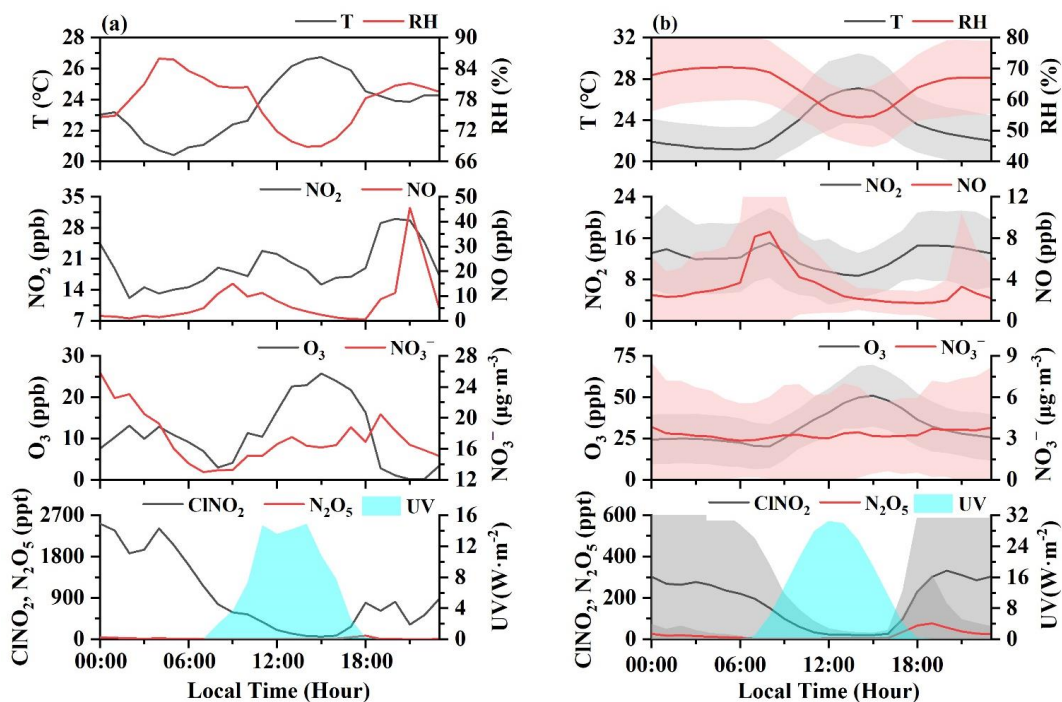
- 471 Wang, Z., Wang, W., Tham, Y. J., Li, Q., Wang, H., Wen, L., Wang, X., and Wang, T.: Fast heterogeneous
472 N₂O₅ uptake and ClNO₂ production in power plant and industrial plumes observed in the nocturnal residual
473 layer over the North China Plain, *Atmos. Chem. Phys.*, 17, 12361-12378, [https://doi.org/10.5194/acp-17-](https://doi.org/10.5194/acp-17-12361-2017)
474 [12361-2017](https://doi.org/10.5194/acp-17-12361-2017), 2017.
- 475 Xia, M., Peng, X., Wang, W., Yu, C., Wang, Z., Tham, Y. J., Chen, J., Chen, H., Mu, Y., and Zhang, C.:
476 Winter ClNO₂ formation in the region of fresh anthropogenic emissions: seasonal variability and insights
477 into daytime peaks in northern China, *Atmos. Chem. Phys.*, 21, 15985-16000, [https://doi.org/10.5194/acp-](https://doi.org/10.5194/acp-21-15985-2021)
478 [21-15985-2021](https://doi.org/10.5194/acp-21-15985-2021), 2021.
- 479 Xia, M., Peng, X., Wang, W., Yu, C., Sun, P., Li, Y., Liu, Y. A. H. C. t. A.-P. O. A. C., Xu, Z., Wang, Z., Xu,
480 Z., Nie, W., Ding, A., and Wang, T.: Significant production of ClNO₂ and possible source of Cl₂ from N₂O₅
481 uptake at a suburban site in eastern China, *Atmos. Chem. Phys.*, 20, 6147-6158, [https://doi.org/10.5194/acp-](https://doi.org/10.5194/acp-20-6147-2020)
482 [20-6147-2020](https://doi.org/10.5194/acp-20-6147-2020), 2020.
- 483 Xue, L. K., Saunders, S. M., Wang, T., Gao, R., Wang, X. F., Zhang, Q. Z., and Wang, W. X.: Development
484 of a chlorine chemistry module for the Master Chemical Mechanism, *Geosci. Model Dev.*, 8, 3151-3162,
485 <https://doi.org/10.5194/gmd-8-3151-2015>, 2015.
- 486 Yan, C., Tham, Y. J., Nie, W., Xia, M., Wang, H., Guo, Y., Ma, W., Zhan, J., Hua, C., and Li, Y.: Increasing
487 contribution of nighttime nitrogen chemistry to wintertime haze formation in Beijing observed during
488 COVID-19 lockdowns, *Nat. Geosci.*, 16, 975-981, <https://doi.org/10.1038/s41561-023-01285-1>, 2023.
- 489 Yi, X., Sarwar, G., Bian, J., Huang, L., Li, Q., Jiang, S., Liu, H., Wang, Y., Chen, H., and Wang, T.:
490 Significant Impact of Reactive Chlorine on Complex Air Pollution Over the Yangtze River Delta Region,
491 China, *J. Geophys. Res. Atmos.*, 128, e2023JD038898, <https://doi.org/10.1029/2023JD038898>, 2023.
- 492 Yun, H., Wang, T., Wang, W., Tham, Y. J., Li, Q., Wang, Z., and Poon, S. C. N.: Nighttime NO_x loss and
493 ClNO₂ formation in the residual layer of a polluted region: Insights from field measurements and an iterative
494 box model, *Sci. Total Environ.*, 622-623, 727-734, <https://doi.org/10.1016/j.scitotenv.2017.11.352>, 2018a.
- 495 Yun, H., Wang, W., Wang, T., Xia, M., Yu, C., Wang, Z., Poon, S. C. N., Yue, D., and Zhou, Y.: Nitrate
496 formation from heterogeneous uptake of dinitrogen pentoxide during a severe winter haze in southern China,
497 *Atmos. Chem. Phys.*, 18, 17515-17527, <https://doi.org/10.5194/acp-18-17515-2018>, 2018b.



498 Zang, H., Zhao, Y., Huo, J., Zhao, Q., Fu, Q., Duan, Y., Shao, J., Huang, C., An, J., Xue, L., Li, Z., Li, C.,
 499 and Xiao, H.: High atmospheric oxidation capacity drives wintertime nitrate pollution in the eastern Yangtze
 500 River Delta of China, *Atmos. Chem. Phys.*, 22, 4355-4374, <https://doi.org/10.5194/acp-22-4355-2022>, 2022.
 501
 502
 503



504
 505 Figure 1. The time series of ClNO_2 , related precursors, and meteorological parameters during the autumn
 506 observation period.



507

508 Figure 2. Diurnal variations of CINO₂ and other related parameters for the highest concentrations of CINO₂

509 (case) on November 28th (a) and the observation-average condition (from 9 October to 5 December) (b).

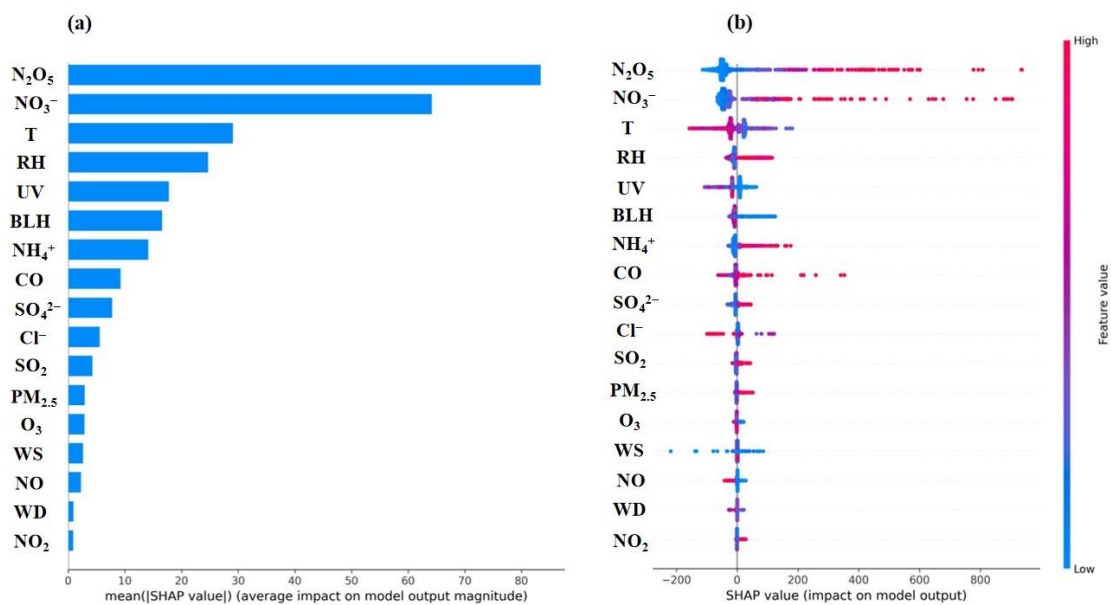
510

511

512

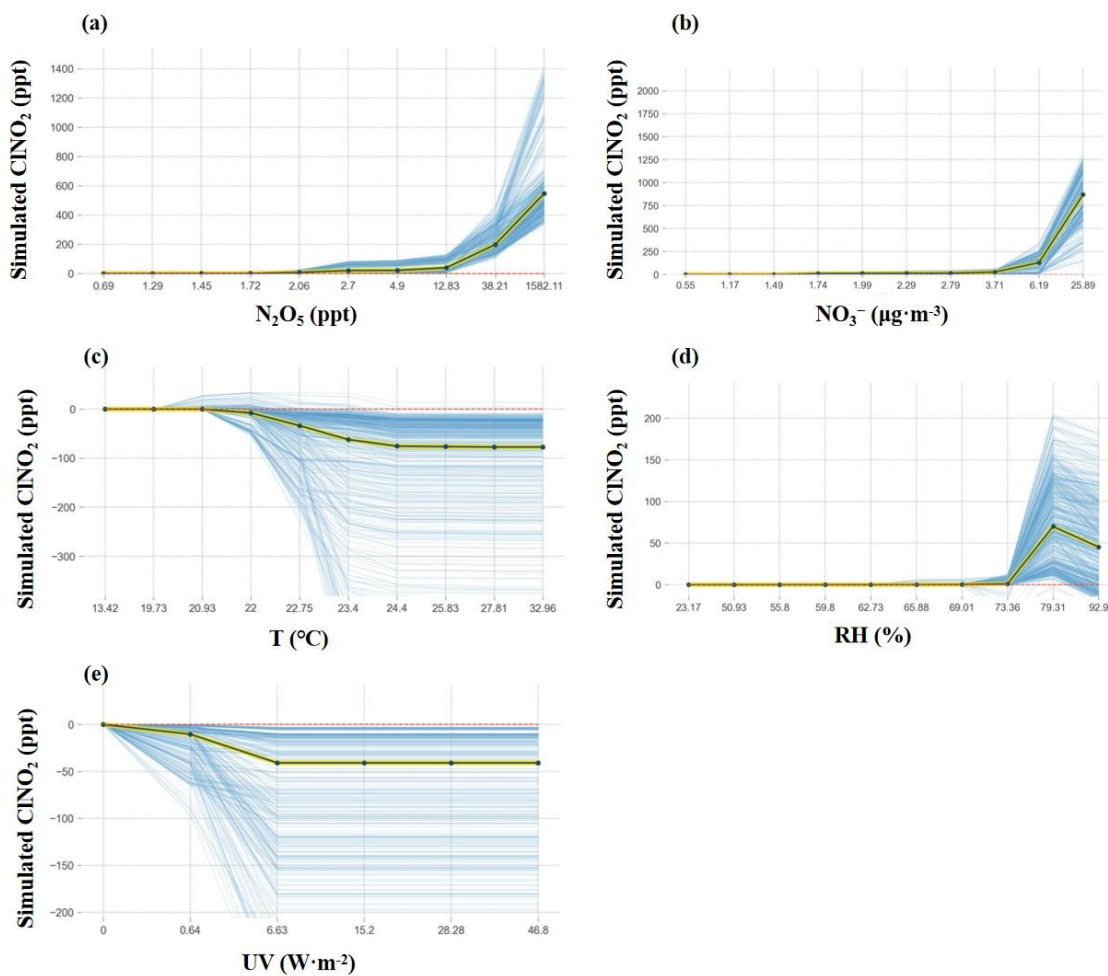
513

514



515

516 Figure 3. Relative importance of each feature to ClNO₂ using XGBoost-SHAP during the autumn
517 observation period. The mean absolute SHAP value (a), summary plot of SHAP values of each feature (b).



518

519 Figure 4. Isolation plots of PDP for N₂O₅ (a), NO₃⁻ (b), T (c), RH (d), and UV (e). The average variations of
520 simulated ClONO₂ with factors' changes spline are indicated by the yellow and black curve, and blue curves
521 presents all situations during the whole observation period.

522

523

524

525

526

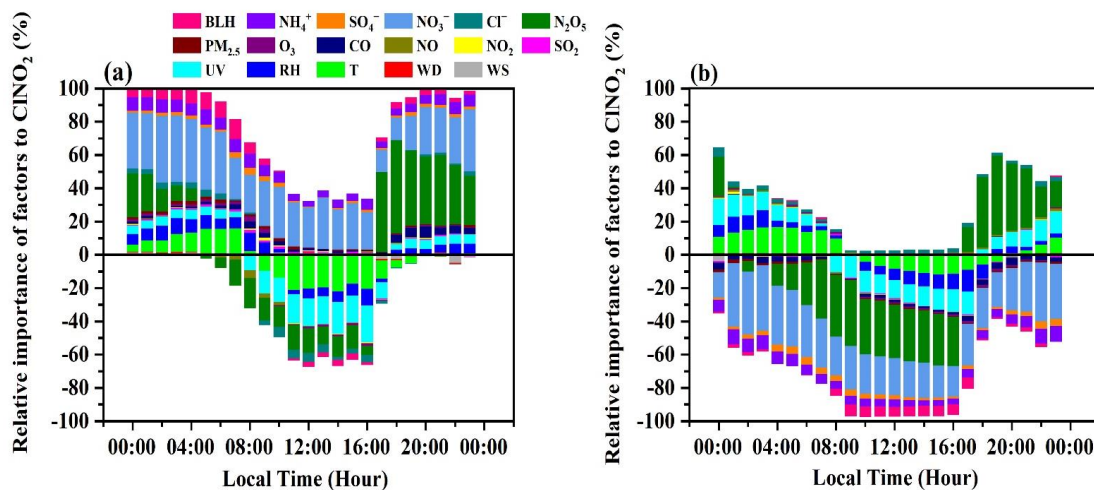
527

528

529



530



531

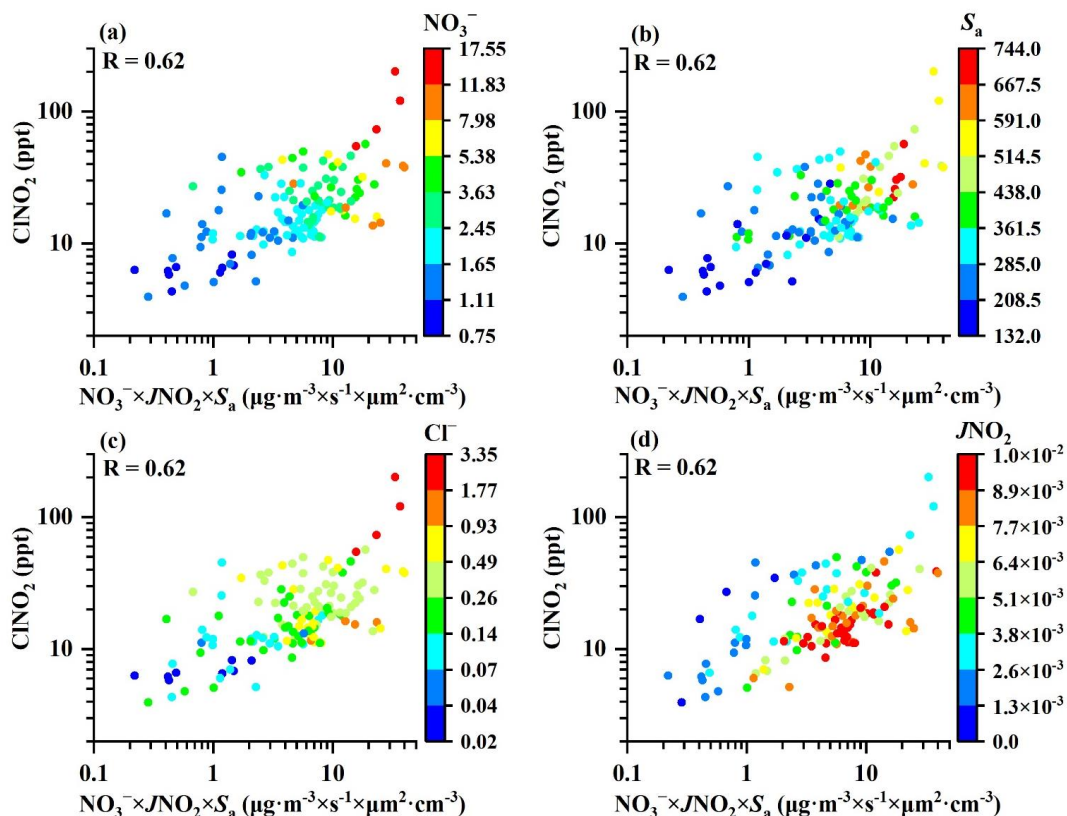
532 Figure 5. The diurnal variations of the relative importance of factors to ClNO₂ based on the SHAP values

533 under the high (> 3.7 µg·m⁻³) (a) and low (< 3.7 µg·m⁻³) (b) ClNO₂ concentrations.

534

535

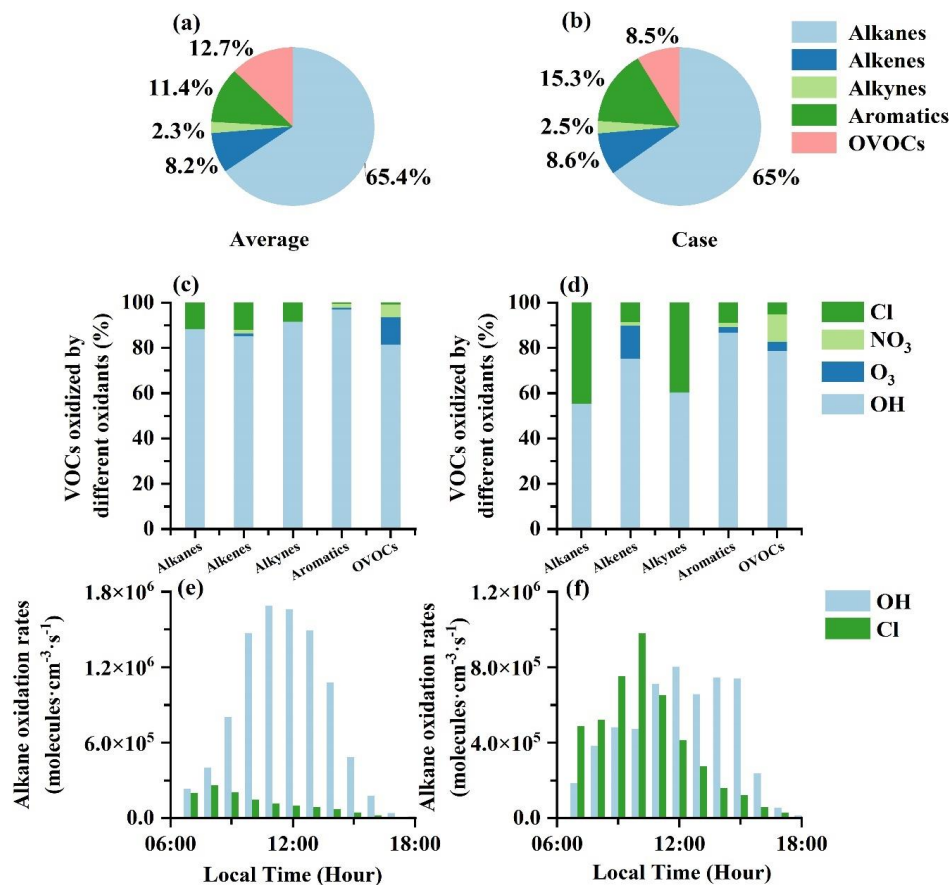
536



537

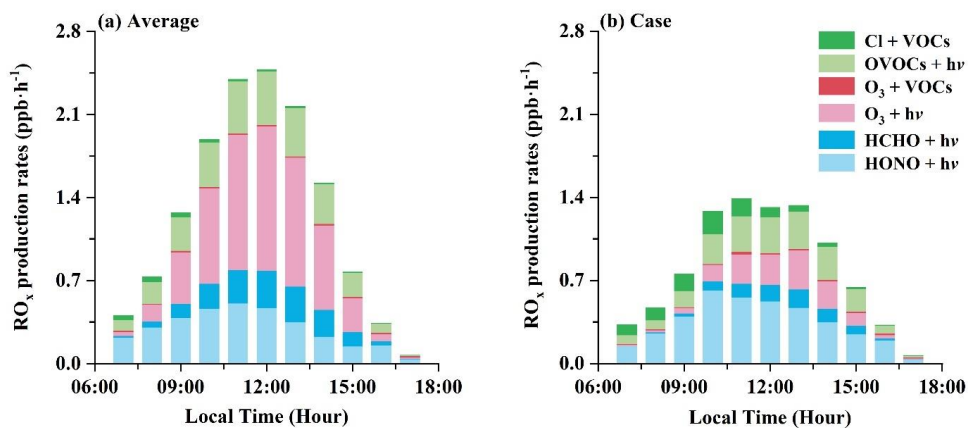
538 Figure 6. The relationship of daytime ClNO_2 concentrations (12:00-15:00 Local Time) and a proxy of nitrate
 539 (NO_3^-) photolysis ($\text{NO}_3^- \times J\text{NO}_2 \times S_a$). The color of the dots respects the NO_3^- (a), S_a (b), Cl^- (c), $J\text{NO}_2$ (d),
 540 respectively.

541



542

543 Figure 7. The impacts of Cl radicals released by ClNO₂ photolysis and other atmospheric oxidants (including
 544 OH, NO₃, and O₃) on VOC oxidation under the observation-average condition and high ClNO₂ case,
 545 respectively. The contributions of different VOC groups oxidized by Cl radical during the observation-
 546 average (a). The contributions of different VOC groups oxidized by Cl radical during the case (b). The
 547 contributions of different atmospheric oxidants (including OH, Cl, NO₃, and O₃) to VOC groups during the
 548 observation-average (c). The contributions of different atmospheric oxidants (including OH, Cl, NO₃, and O₃)
 549 to VOC groups during the case (d). Comparisons of alkane oxidation rates (molecules·cm⁻³·s⁻¹) by OH and
 550 Cl radical during the observation-average (e). Comparisons of alkane oxidation rates by OH and Cl radical
 551 (molecules·cm⁻³·s⁻¹) during the case (f).



552

553 Figure 8. The contributions of different production pathways to RO_x production rates under the observation-

554 average condition (a) and high ClNO₂ case (b), respectively.

555

556

557

558

559

560

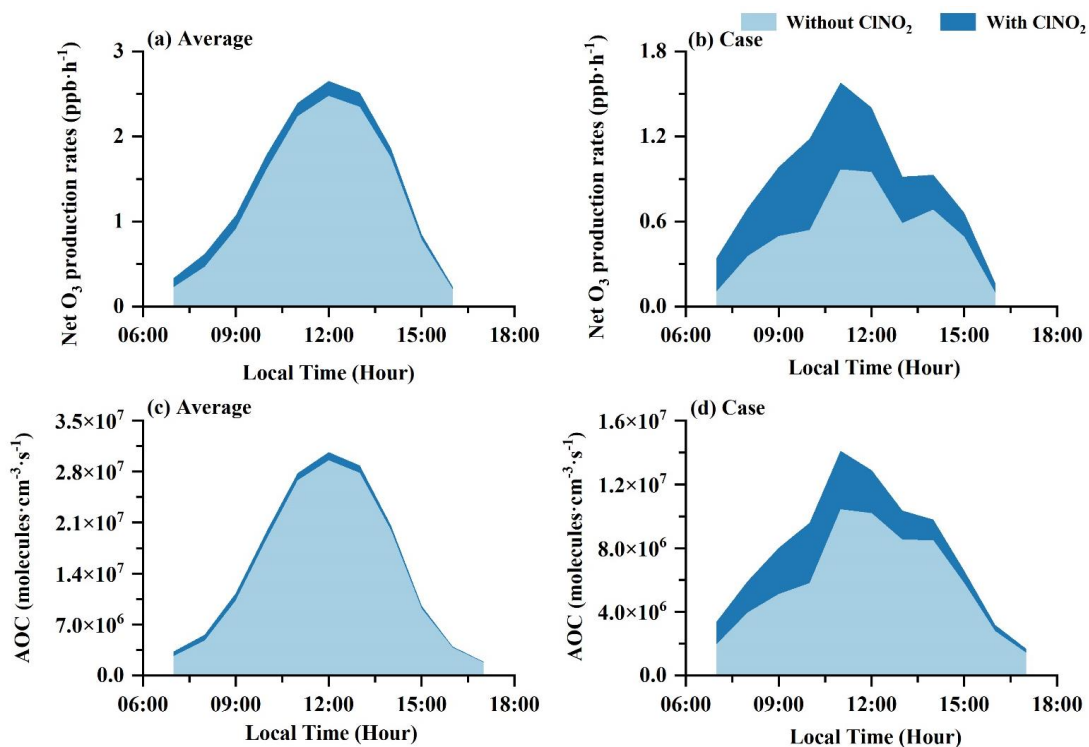
561

562

563

564

565



566

567 Figure 9. The impacts of Cl radicals released by ClNO₂ photolysis on net O₃ production rates and the AOC
568 levels under the observation-average condition (a, c) and high ClNO₂ case (b, d), respectively.

569

570

571

572

573

574

575

576

577

578

579

580

581

582



583 Table 1. Relative importance of Cl, OH, and O₃ to the daytime oxidation of VOC groups (including alkanes,
584 alkenes, alkynes, aromatics, and OVOCs) around the world (Xue et al., 2015; Bannan et al., 2015; Bannan et
585 al., 2017; Rutherford et al., 1995; Fraser et al., 1997).

	Xiamen (average)	Xiamen (case)	Hong Kong (max)	London (average)	Weybourne (average)	Boston	LA
Alkane Cl%	11.7	44.8	53.0	3.5	1.0	8.5	9.9
Alkane OH%	88.3	55.2	47.0	96.5	99.0	91.5	90.1
Alkane O ₃ %	-	-	-	-	-	-	-
Alkene Cl%	12.2	8.7	14.0	0.6	0.4	0.3	0.3
Alkene OH%	85.0	75.2	81.0	77.9	78.3	33	31.3
Alkene O ₃ %	1.2	14.7	5.0	21.5	21.4	66.7	68.4
Alkyne Cl%	8.5	40.0	-	7.0	2.6	8.7	8.7
Alkyne OH%	91.5	60.0	-	91.8	96.7	89.7	89.7
Alkyne O ₃ %	-	-	-	1.2	0.7	1.6	1.6
Aromatics Cl%	0.7	9.1	11.0	-	-	-	-
Aromatics OH%	97.0	86.6	89.0	-	-	-	-
Aromatics O ₃ %	0.7	2.6	-	-	-	-	-
OVOCs Cl%	0.9	5.2	6.0	-	-	-	-
OVOCs OH%	81.4	78.7	85.0	-	-	-	-
OVOCs O ₃ %	12.0	3.9	-	-	-	-	-

586

587

588

589

590

591

592

593

594

595

596

597

598

599



600

601 Table 2. The impacts of ClNO₂ photolysis on RO_x (OH, HO₂, and RO₂) levels, P(RO_x), and P(O₃) around the
 602 world (Xia et al., 2021; Wang et al., 2022; Tham et al., 2016; Wang et al., 2016; Xue et al., 2015; Bannan et
 603 al., 2017; Jeong et al., 2019).

Study Area	Season	OH	HO ₂	RO ₂	P(RO _x)	P(O ₃)
Xiamen (average)	Autumn	3.7%	7.1%	10.3%	4.9%	6.7%
Xiamen (case)	Autumn	17.9%	34.6%	54.3%	23.8%	41.7%
Wangdu/Beijing/Mt. Tai	Winter	15.0%–22.0%	24.0%–31.0%	36.0%–52.0%	1.3%–3.8%	1.3%–6.2%
Heshan	Autumn	1.5%–2.6%	1.9%–4.6%	3.0%–6.8%	< 2.2%	1.0%–4.9%
Wangdu	Summer	-	-	-	10%–30%	3.0%–13.0%
Mt. Tai Mo Shan, Hong Kong	Winter	40.0%–77.0%	53.0%–106.0%	-	-	11.0%–41.0%
Hok Tsui, Hong Kong	Summer	6.6%	12.2%	45.1%	-	10.3%
Weybourne	Spring	5.0%	7.0%	9.0%	-	-
Seoul	Spring	-	-	-	-	1.0%–2.0%

604